Original Article

JCBFM

Journal of Cerebral Blood Flow & Metabolism
2020, Vol. 40(5) 1012–1020

DOI: 10.1177/0271678X19853117
journals.sagepub.com/home/jcbfm
SAGE

Comparison of high and low molar activity TSPO tracer [^{18}F]F-DPA in a mouse model of Alzheimer's disease

Thomas Keller[1,2], Francisco R López-Picón[3,4], Anna Krzyczmonik[1,2], Sarita Forsback[1,2], Jatta S Takkinen[3,4], Johan Rajander[5], Simo Teperi[6], Frédéric Dollé[7], Juha O Rinne[1], Merja Haaparanta-Solin[3,4] and Olof Solin[1,2,5]

Abstract

[^{18}F]F-DPA, a novel translocator protein 18 kDa (TSPO)-specific radioligand for imaging neuroinflammation, has to date been synthesized with low to moderate molar activities (A_m's). In certain cases, low A_m can skew the estimation of specific binding. The high proportion of the non-radioactive component can reduce the apparent-specific binding by competitively binding to receptors. We developed a nucleophilic synthesis of [^{18}F]F-DPA resulting in high A_m (990 ± 150 GBq/μmol) and performed in vivo comparison with low A_m (9.0 ± 2.9 GBq/μmol) [^{18}F]F-DPA in the same APP/PS1-21 and wild-type mice (injected masses: 0.34 ± 0.13 μg/kg and 38 ± 15 μg/kg, respectively). The high level of microgliosis in the APP/PS1-21 mouse model enables good differentiation between diseased and healthy animals and serves better to distinguish the effect of differing A_m on specific binding. The differing injected masses affect the washout profile and shape of the time–activity curves. Ratios of standardized uptake values obtained with high and low A_m [^{18}F]F-DPA demonstrate that there is a 1.5-fold higher uptake of radioactivity in the brains of APP/PS1-21 animals when imaging is carried out with high A_m [^{18}F]F-DPA. The differences between APP/PS1-21 and wild-type animals showed higher significance when high A_m was used.

Keywords

APP/PS1-21, fluorine-18, Neuroinflammation, positron emission tomography, TSPO

Received 11 December 2018; Accepted 7 April 2019

Introduction

Positron emission tomography (PET) is an important diagnostic technique for the visualization of functional processes in the human body by monitoring the distribution and accumulation of tracers labelled with a radioactive isotope. In PET, it is the intention to image a system that is not being perturbed by external factors during the course of the scan. Since most radiotracers are derived from bioactive or pharmaceutical molecules, it is crucial to keep the administered mass as low as possible in order to avoid any unwanted pharmacological effects. At the same time, it is essential to inject sufficient amount of radioactivity to allow for accurate scanning of the subject. Hence, a sufficiently high molar activity (A_m, defined as the amount of radioactivity in a certain quantity of tracer) is a crucial characteristic for the use of a particular radiotracer. Low A_m can pose a problem in cases of low target abundance since there will be competition between

[1]Radiopharmaceutical Chemistry Laboratory, Turku PET Centre, University of Turku and Turku University Central Hospital, Turku, Finland
[2]Department of Chemistry, University of Turku, Turku, Finland
[3]MediCity Research Laboratory, University of Turku, Turku, Finland
[4]PET Preclinical Imaging Laboratory, Turku PET Centre, University of Turku, Turku, Finland
[5]Accelerator Laboratory, Turku PET Centre, Åbo Akademi University, Turku, Finland
[6]Department of Biostatistics, University of Turku, Turku, Finland
[7]CEA, I2BM, Service Hospitalier Frédéric Joliot, Orsay, France

Corresponding author:
Olof Solin, Turku PET Centre, University of Turku, Kiinamyllynkatu 4-8, FI-20520 Turku, Finland.
Email: olof.solin@abo.fi

the radioactively labelled and non-radioactive analogues, with the so-called "cold" compound blocking the receptors to occupancy by the radioactively labelled molecules. In human studies and in cases of high target abundance, A_m is not a crucial factor. This is supported, for example, by the continued use of [^{18}F]F-DOPA[1] which is produced in relatively low A_m by the electrophilic fluorination approach as well as by the work of Fujimura et al.[2] which showed no significant difference between the use of high and ultra-high A_m [^{11}C]raclopride for imaging the dopamine D_2 receptor. Preclinical work in rodents requires administration of radioactivity at a higher proportion relative to the body weight that clinical studies. Due to this there is a tendency to push the limit of the injected mass and hence A_m plays a more critical role in the imaging of small animals than it does in the imaging of humans.

Fluorine-18, one of the most commonly used radionuclides in PET, has a suitably long half-life ($t_{½} = 109.8$ min) to allow for relatively lengthy syntheses and even distribution to PET centres without an on-site cyclotron. While fluorine is not found in many naturally occurring bioactive molecules that would be suitable for labelling, nowadays fluorine can be found in approximately 20% of all the new pharmaceutical compounds coming to the market.[3–5] The increase in recent years of the numbers of fluorine-containing radiopharmaceuticals can be attributed to the numerous useful properties, such as increased lipophilicity and metabolic stability, which the fluorine atom can impart to the molecule. The shortcoming of fluorine-18 for tracer synthesis lies in the possible labelling strategies. While in non-radioactive chemistry, the electrophilic and nucleophilic fluorination methods are complementary processes that are used indiscriminately, the chemistry of fluorine-18 is dominated by the latter approach. This can be attributed to the relatively low A_m's obtained by the traditional cyclotron-methods for the production of electrophilic [^{18}F]F_2 (^{20}Ne(d,α)^{18}F and ^{18}O(p,n)^{18}F which lead to A_m's of 0.1 GBq/μmol[6] and 1.3 GBq/μmol,[7] respectively) and the requirement of specialized equipment for the post-target production synthesis of [^{18}F]F_2 gas which leads to an A_m of 55 GBq/μmol by the high voltage discharge method[8] and 10.3 ± 0.9 GBq/μmol by the vacuum UV-photon illumination approach.[9] Unlike the electrophilic approach, for the nucleophilic labelling method, the A_m is not well controlled and the reported A_m's can range from 1 to 10 GBq/μmol all the way to multi-TBq/μmol.

Despite the low A_m associated with electrophilic ^{18}F-fluorination, this labelling strategy has for a long time been the most facile methodology for the ^{18}F-fluorination of electron rich aromatic rings. As such, it has been used in the synthesis of tracers such as [^{18}F]EF5,[10] [^{18}F]FDOPA,[1] [^{18}F]CFT,[11] and most recently [^{18}F]F-DPA.[12]

[^{18}F]F-DPA, a relatively new analogue of [^{18}F]DPA-714, was produced for preclinical evaluation by an electrophilic ^{18}F-fluorination approach using post-target produced [^{18}F]F_2-derived [^{18}F]Selectfluor bis(triflate) with A_m's of 7.8 ± 0.5 GBq/μmol. It has been shown to be more stable with respect to metabolism thanks to its labelling position directly on the aromatic ring,[12] and its specificity for the target was confirmed by pre-treatment with PK11195.[13,14] Due to the favourable characteristics of [^{18}F]F-DPA, much attention has been devoted to the development of a nucleophilic synthesis.[14–16] Nevertheless, the A_m of this promising new 18 kDa translocator protein (TSPO)-specific tracer has to date been approximately 10-fold lower than the routinely used [^{18}F]DPA-714[1,2] which is also synthesized by a nucleophilic approach.

Reported herein is the synthesis of high A_m [^{18}F]F-DPA by a copper-mediated nucleophilic ^{18}F-fluorination methodology which has been developed by modifying previously reported procedures.[17,18] The transgenic (TG) APP/PS1-21 mouse model of Alzheimer's disease (AD), which was previously studied using [^{18}F]DPA-714[1,9] and [^{18}F]F-DPA,[13] has been employed together with wild-type (WT) mice to evaluate the efficacy of high A_m [^{18}F]F-DPA for the detection of TSPO-overexpression. Most importantly, the in vivo behaviour of high A_m [^{18}F]F-DPA, produced by the nucleophilic route, has been directly compared to that of the lower A_m [^{18}F]F-DPA, produced by the electrophilic labelling method. This was achieved by imaging the same animals with [^{18}F]F-DPA made by both of the synthesis routes, with the premise that the differing A_m's and injected masses will have a pronounced effect on the tracer uptake and kinetics.

Materials and methods

All organic solvents were HPLC-grade and purchased from Sigma-Aldrich (Steinheim, Germany). Potassium carbonate, potassium oxalate, dimethyl acetamide and Tetrakis(pyridine)copper(II) triflate were also purchased from Sigma-Aldrich. Kryptofix 222 (4,7,13,16,21,24-hexaoxa-1,10-diazabicyclo[8.8.8]hexacosane) and sodium dihydrogen phosphate were purchased from Merck KGaA (Darmstadt, Germany). Ammonium acetate was bought from Alfa Aesar (Karlsruhe, Germany). Ethanol, saline (0.9% aq. NaCl) and phosphate buffer (0.1 M aq. Na_3PO_4) for formulation were purchased from Berner Oy (Helsinki, Finland), B. Braun Medical Oy (Helsinki, Finland) and Turku University Hospital Pharmacy (Turku, Finland), respectively. Oxygen-18-enriched

Hyox water, for fluorine-18-production, was purchased from Rotem Industries Ltd. (Arava, Israel). All gases were supplied by AGA, Linde group (Espoo, Finland).

For the product of the nucleophilic fluorination reaction, numerous preparative HPLC systems were tested, of these, the systems that provided the best separation are described below.

HPLC system A for purification, consisted of a Merck Hitachi L-6200 pump with a L-7400 UV detector and a NaI(TI) scintillator detector or a Jasco PU-2089 pump and a UV detector. The column used was a Waters X-Terra Prep RP18 (7 μm, 7.8 × 300 mm) column (Waters Corporation, Milford MA, USA) and the eluent system: 0 to 5 min; 100% aqueous: $CH_3CO_2NH_4$ (0.1 M, pH 8.5), 5 to 55 min; 0 to 22% organic: CH_3CN, 55 min onwards; isocratic eluent system 78% aqueous and 22% organic. The flowrate was 6 mL/min during the whole method. Using these conditions, [^{18}F]F-DPA had a retention time of 115 min.

HPLC system B for analysis consisted of a Merck Hitachi LaChrom 7000 system with Merck Hitachi D-7000 HPLC System Manager software (version 3.1.1), or a VWR Hitachi LaChrom Elite system with EXChrom Elite Client/Server software (version 3.1.6). Analyses were carried out with a wavelength of 254 nm and the radioactivity was detected with a NaI(TI) scintillator detector. The system employed a Merck Chromolith Performance RP-18e (10 μm, 4.6 × 100 mm) column (Merck KGaA, Darmstadt, Germany) with an eluent system consisting of 0- to 5-min 100% aq. NaH_2PO_4 (0.025 M, pH 3.5), 5- to 25-min 0 to 22% CH_3CN, 25 min onwards 22% CH_3CN and a flowrate of 2 mL/min. Using these conditions, [^{18}F]F-DPA showed a retention time of 64.2 min.

HPLC purification and analysis of [^{18}F]F-DPA$_E$ was performed according to previously described procedure.[12]

Fluorine-18 was produced using the previously described procedures.[12]

Nucleophilic ^{18}F-fluorination procedure

Aqueous ^{18}F-fluoride from the cyclotron-target was added to a reaction vessel containing Kryptofix 222 [6.2 ± 0.2 mg (16.2 ± 0.4 μmol)] in CH_3CN (100 μL) and K_2CO_3 (20 μmol). CH_3CN (0.5 mL) was then added and azeotropic distillation was carried out for 8 min at a temperature of 100°C under a helium flow. Two further additions of CH_3CN (2 × 0.5 mL) were made, each followed by a 5-min evaporation.

On cooling, $Cu(OTf)_2(pyr)_4$ [14.3 ± 2.0 mg (21.1 ± 0.3 μmol)] in CH_3CN (0.5 mL) was added to the dry Kryptofix 222/K^+[^{18}F]F^- complex, and the reaction mixture was stirred at room temperature for 10 min. Following this, the solvent was evaporated and the precursor, 4.7 ± 0.3 mg (7.5 ± 0.5 μmol), in DMA (0.5 mL) was added to the reaction mixture, and the reaction mixture was heated under reflux for 10 min. After the reaction, half of the solvent was evaporated and the remaining reaction mixture was diluted with aqueous $CH_3CO_2NH_4$ (0.1 M, pH 8.5, 1.5 mL) and purified using HPLC system A.

After preparative HPLC, the fraction containing the product was collected, diluted with water (25 mL), and passed over a Waters Sep-Pak Light tC18 cartridge (Waters Corporation, Milford, MA, USA), thereby trapping the radioligand. The cartridge was then washed with water (25 mL). [^{18}F]F-DPA was finally eluted using ethanol (200 μL) and further diluted with 0.1 M phosphate buffer to give a 10% ethanolic solution, suitable for intravenous injection.

Electrophilic synthesis of [^{18}F]F-DPA

The electrophilic syntheses of [^{18}F]F-DPA were performed according to previously described procedures (Figure 1).[12]

Animals and ethical statement

This study was performed on 9-month-old TG APP/PS1-21 AD-model mice (TG, n = 3, two males and one female) and WT mice (n = 3, one male and two females). The Aβ42-driven cerebral amyloidosis starts at 6 to 8 week.[20] β immunoreactive plaques develop progressively in the neocortex and hippocampus (HIPP) and are associated with dystrophic neurites and gliosis.[20] APP/PS1-21 mice were originally provided by KOESLER (Rottenburg, Germany) and were further bred in the Central Animal Laboratory of University of Turku with C57BL/6Cn mice. The guidelines of the International Council of Laboratory Animal Science were followed with regard to animal care. All animals were group housed under standard conditions (temperature: 21°C ± 3°C, humidity: 55 ± 15%, lights on from 6:00 a.m. until 6:00 p.m.) at the Central Animal Laboratory, University of Turku and had ad libitum access to soy-free chow (RM3 (E) soya-free, 801710, Special Diets Service) and tap water.

The study was performed in accordance with the ARRIVE guidelines and was approved by the Animal Experiment Board of the Province of Southern Finland (license numbers: ESAVI/4660/04.10.07/2016).

In vivo PET/computed tomography imaging and analysis

For in vivo comparison, PET imaging was performed on TG (n = 3, two males and one female, weight: 26.5 ± 3.1 g) and WT mice (n = 3, one male and two females, weight: 38.1 ± 1.7 g) which were imaged with

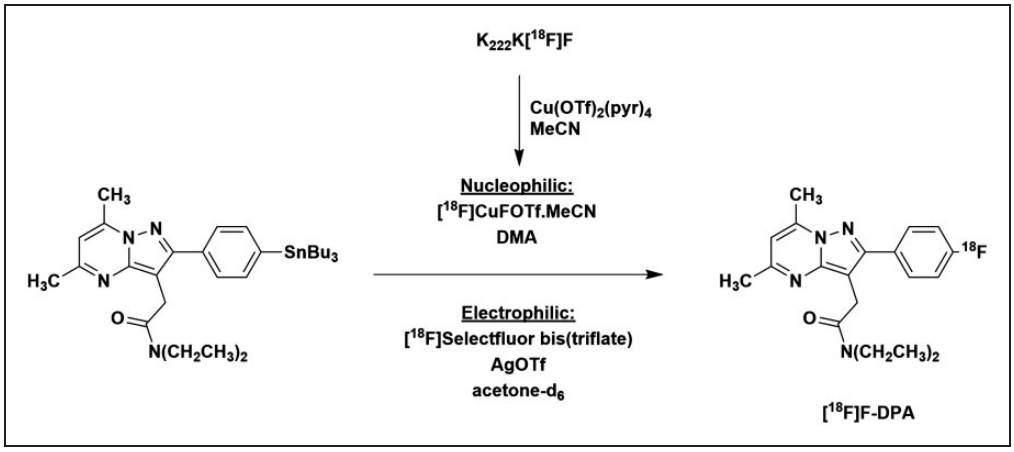

Figure 1. Synthesis of [^{18}F]F-DPA from the stannylated precursor by copper-mediated nucleophilic [^{18}F]fluorination and electrophilic [^{18}F]fluorination using post-target produced [^{18}F]F_2 derived [^{18}F]Selectfluor bis(triflate).

[^{18}F]F-DPA$_E$ and [^{18}F]F-DPA$_N$ a week apart. On the first day, the mice were imaged using [^{18}F]F-DPA$_E$ (6.81 ± 0.08 MBq, 38 ± 15 μg/kg, A_m at time of injection was 2.25 ± 0.96 GBq/μmol). A week later, on the second day of imaging, [^{18}F]F-DPA$_N$ (6.96 ± 0.23 MBq, 0.34 ± 0.13 μg/kg, A_m at time of injection was 260 ± 110 GBq/μmol) was used.

Imaging was carried out using the Inveon multimodality PET/computed tomography scanner (Siemens Medical Solutions, Knoxville, TN, USA), this together with the subsequent image analysis was carried out according to the previously described procedures.[12] Standardized volumes of interest (VOIs) were placed in the parietotemporal cortex (PTC), HIPP, and whole brain (WB) with Inveon Research Workplace 3.0 (Siemens Medical Solutions) using the MRI template as anatomic reference (McKnight Brain Institute, MRM NAt Mouse Brain Database. Mouse MRI brain template. http://brainatlas.mbi.ufl.edu/Database/ (2005, accessed 17 May 2013)).

Standardized uptake values (SUVs) were calculated as the ratio of the tissue radioactivity concentration (Bq/mL) and the injected activity (Bq) (decay corrected to the same time) divided by the body weight (g).

Ex vivo brain autoradiography

Following the in vivo studies using [^{18}F]F-DPA$_N$, while still under deep anaesthesia, the mice were sacrificed by cardiac puncture. Transcardial perfusion with saline was conducted rapidly in order to eliminate blood from the brain. Once the brain was removed, coronal brain sections of 20 μm were prepared, scanned and analysed as previously described.[13] Regions of interest (ROIs) were drawn on the PTC, HIPP as well as the frontal cortex (FC), striatum, thalamus and hypothalamus (HYP). The ROIs were calculated as photostimulated intensity/area − background (PSL/mm^2) and presented as ROI/HYP ratios. The HYP was used as the reference region for ex vivo autoradiography since it has previously been demonstrated that it is relatively clear of pathology and hence shows low tracer uptake in this particular model of disease.[13]

Radiometabolite analyses of [^{18}F]F-DPA$_N$

For radiometabolite analysis of [^{18}F]F-DPA$_N$, the blood and brain samples were taken from the same mice used in the imaging studies. The preparation of samples and thin-layer chromatographic (TLC) analysis was carried out according to previously published methods.[12]

Statistical methods

Data are given as mean ± standard deviation. Differences between the averaged SUVs for TG and WT animals were tested using the two-tailed unpaired t-test. In the case of the ex vivo autoradiography ratios, the differences were tested between ROI/HYP ratios for TG and WT animals when they were imaged with either high or low A_m [^{18}F]F-DPA as well as between the ROI/HYP for TG animals when imaging was carried out with high and low A_m [^{18}F]F-DPA and likewise for WT animals. Differences were considered significant if the P value was less than 0.05. All statistical analyses were performed using the Graph-Pad Prism program (version 6.04; GraphPad Software).

Results

Radiochemistry

These results from the electrophilic syntheses, $15.9 \pm 4.3\%$ radiochemical yield (decay corrected to

end of bombardment (EOB) and calculated from [^{18}F]Selectfluor *bis*(triflate)) and an A_m of 9.0 ± 2.9 GBq/μmol, are on par with those reported previously.[12]

The initially attempted, one-pot nucleophilic fluorination labelling reaction yielded none of the [^{18}F]F-DPA product. The product was, however, successfully synthesized when the [^{18}F]fluoride was premixed with copper triflate in CH_3CN and the solvent was changed to DMA for the reaction to produce [^{18}F]F-DPA (Figure 1). By this procedure, [^{18}F]F-DPA$_N$ was obtained in $11.4 \pm 1.0\%$ radiochemical yield (determined by radioHPLC) with A_m of 990 ± 150 GBq/μmol (decay corrected to EOB).

In vivo

The time–activity curves (TACs) for the PTC, HIPP and WB (Figure 2) show that [^{18}F]F-DPA$_E$ has a sharp initial uptake peak and fast subsequent wash out. The initial uptake of high A_m [^{18}F]F-DPA$_N$ reaches a similar level as [^{18}F]F-DPA$_E$, for TG and WT animals, respectively. However both the initial uptake and subsequent washout of the radionuclide are slower for the high A_m [^{18}F]F-DPA$_N$. This difference between [^{18}F]F-DPA$_N$ and [^{18}F]F-DPA$_E$ is apparent in both the TG as well as WT animals.

Whereas the [^{18}F]F-DPA$_E$ TAC reaches an approximate plateau at around 20- to 40-min postinjection, the [^{18}F]F-DPA$_N$ does not reach a similar plateau even by the end of the 60-min scan. Nevertheless, when using [^{18}F]F-DPA$_N$, significant differences were detected between the TG and WT in all of the brain areas studied already during the 20 to 40 min window after injection. With [^{18}F]F-DPA$_E$, differences between TG and WT were only found to be significant in the PTC and HIPP. Regardless of the A_m of the tracer used, when present, the differences between the TACs of TG and WT animals represented more significant differences when they were averaged for the 20- to 40-min period compared to the 40- to 60-min interval.

Ex vivo

The animals were imaged in vivo with both tracers, and they were sacrificed for brain autoradiography after they were imaged with [^{18}F]F-DPA$_N$. For the comparison, the brain ROI/HYP autoradiography obtained with the high A_m [^{18}F]F-DPA$_N$ was compared with the data previously obtained using [^{18}F]F-DPA$_E$.[13] With the exception of the FC, there are no significant differences between the ROI/HYP ratios of TG mice. Highly significant differences can be seen between WT and TG animals, in all the brain regions studied, when they are imaged with either [^{18}F]F-DPA$_N$ or [^{18}F]F-DPA$_E$ (Figure 3).

In all of the brain regions studied, there is no significant difference between the data of the WT animals obtained using [^{18}F]F-DPA produced by either approach.

RadioTLC metabolite analysis

RadioTLC analysis of brain homogenate showed that, at the end of the scan, more than 99% of the remaining activity could be attributed to the unchanged [^{18}F]F-DPA$_N$. In the plasma, the unchanged [^{18}F]F-DPA$_N$

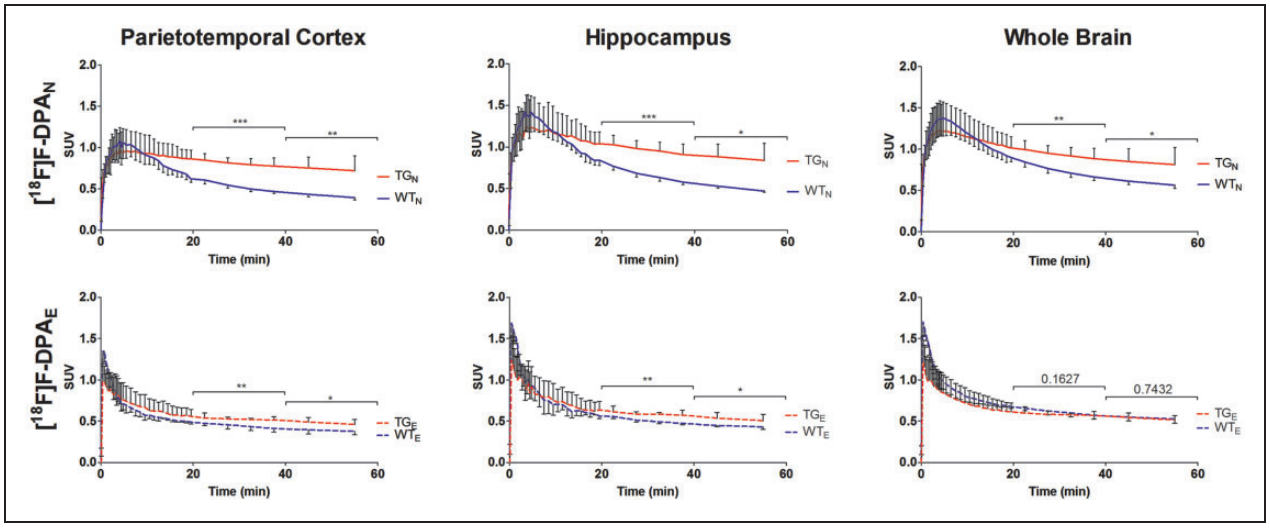

Figure 2. Time–activity curves derived from the parietotemporal cortex, hippocampus and whole brain VOIs for TG and WT mice at 9 months obtained using [^{18}F]F-DPA$_N$ and [^{18}F]F-DPA$_E$ ($n = 3$ per group). * are used to denote the level of significance between WT and TG for SUVs averaged for the 20- to 40-min and 40- to 60-min time intervals (*$P < 0.05$,**$P < 0.01$, ***$P < 0.001$).

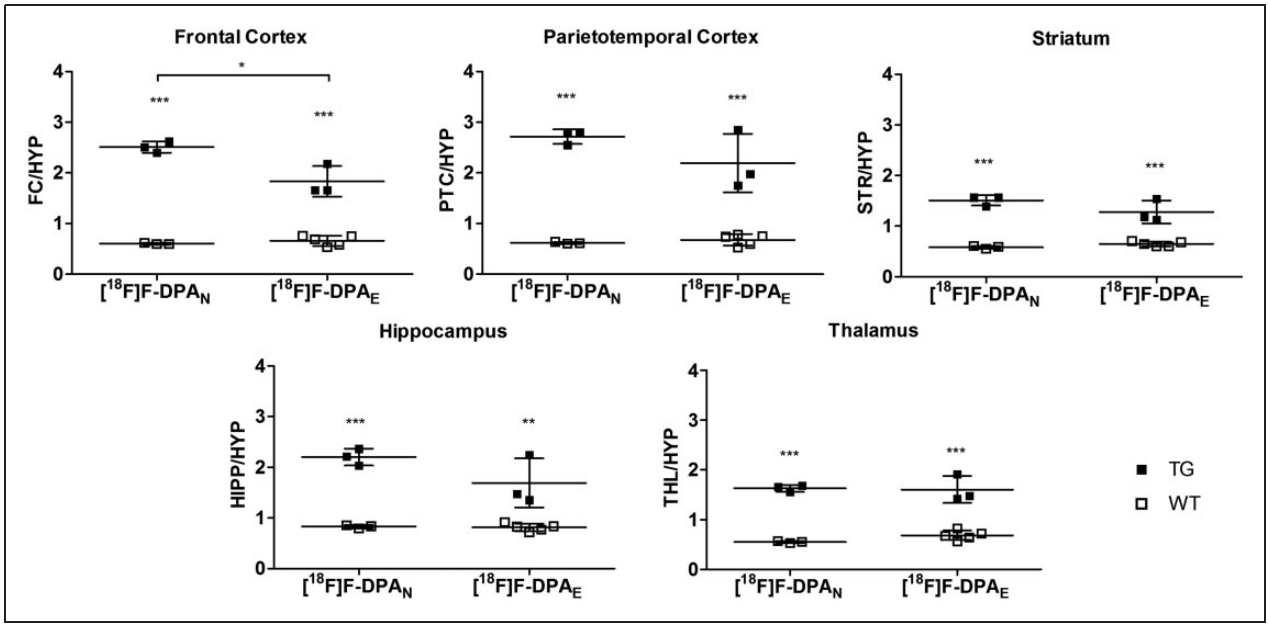

Figure 3. Ex vivo brain autoradiography ratios of 9 month TG and WT animals obtained with high and low A_m [^{18}F]F-DPA (n = 3–5). The animals were sacrificed after a 60-min PET scan was carried out, autoradiography imaging was performed immediately thereafter. The results are presented as ROI to HYP ratios the FC, PTC, STR, HIPP and THL. *$P < 0.05$, ***$P < 0.01$, ***$P < 0.001$. HYP: hypothalamus; FC: frontal cortex; PTC: parietotemporal cortex; STR: striatum; HIPP: hippocampus; THL: thalamus.

accounted for 76.5 ± 2.4% of the remaining activity 60 min after injection. These findings are in line with those previously reported for radioTLC analyses of brain homogenate and plasma from mice injected with [^{18}F]F-DPA$_E$.[13] In this previous study, the unchanged tracer accounted for 99% and 70% of the remaining radioactivity in the brain and plasma, respectively, at 60 min after injection.

Discussion

Initial nucleophilic syntheses of [^{18}F]F-DPA$_N$ were attempted as one-step reactions employing either MeCN or DMA as the reaction. However, neither of these reactions afforded the desired [^{18}F]F-DPA product. Premixing the [^{18}F]fluoride with copper (II) triflate in acetonitrile for 10 min, evaporating the acetonitrile and subsequently performing the labelling reaction on the stannyl in DMA yielded the desired [^{18}F]F-DPA$_N$. As previously hypothesized and investigated by Gamache et al.,[18] acetonitrile plays a critical role in mediating the reaction, most likely by stabilizing a [^{18}F]CuF(OTf) intermediate through ligation. In contrast to the work of Gamache et al., the subsequent labelling reaction did not proceed when using acetonitrile as the reaction solvent; however, when DMA, which allowed for a higher reaction temperature, was used, the product was obtained in 11.4 ± 1.0% radiochemical yield (determined by radioHPLC).

As expected, the in vivo TACs (Figure 2) show that there is significantly higher tracer binding and retention in the brains of TG mice compared to the WT controls. A distinct difference can be seen between the shapes of the TACs when the tracer was synthesized by either the nucleophilic or electrophilic approach. Since the amount of radioactivity administered is essentially same (approximately 6.9 MBq), we can conclude that this derives from the respective A_m's and injected masses of the [^{18}F]F-DPA which, due to the different labelling approaches, vary by more than a factor of 100. The [^{18}F]F-DPA$_E$ contains a relatively high quantity of non-radioactive F-DPA; hence, the washout profile is similar to that observed for other TSPO-specific low A_m tracers such as [^{18}F]PK14105 (A_m = 7.4 GBq/μmol at EOB),[22] for studies when the animal is pretreated with a competitively binding ligand[23–26] or when the non-radioactively labelled ligand is co-injected with the tracer.[23,27,28] The non-radioactive F-DPA present in the [^{18}F]F-DPA$_E$ competitively binds to and occupies a large proportion of the TSPO. In the case of [^{18}F]F-DPA$_N$, the injected mass is very low by comparison and hence a higher proportion of the radioactively labelled [^{18}F]F-DPA can bind to TSPO. The high initial binding is hence followed by the typical washout[12] of a high A_m TSPO tracer. In the previously reported study employing [^{18}F]F-DPA produced by a nucleophilic route from an iodonium ylide,[14] the TACs (for the WB) had a shape that resembled something in

between the TACs reported here for [^{18}F]F-DPA$_N$ and [^{18}F]F-DPA$_E$. This results from the fact that the A_m was approximately 100 GBq/μmol. This A_m, and by extension the injected mass, is around 10 times higher than that of [^{18}F]F-DPA$_E$ and 10 times lower than that of [^{18}F]F-DPA$_N$. This comparison further lends weight to the hypothesis that the washout profile of the radioactivity is highly dependent on the amount of cold compound that is co-administered.

The significances of the differences between SUVs of WT and TG animals averaged over the different time intervals (20–40 and 40–60 min) in the various brain regions are also shown in Figure 2. These demonstrate that there are significant differences in [^{18}F]F-DPA uptake between TG and WT animals in all of the brain regions studied, with the exception of the WB when imaging was carried out with [^{18}F]F-DPA$_E$. When significant, the differences between the averaged SUVs for TG and WT mice show greater significance during the 20- to 40-min interval and when imaging was carried out with [^{18}F]F-DPA$_N$.

Figure 4 shows the plots of the [^{18}F]F-DPA$_N$/[^{18}F]F-DPA$_E$ SUV ratios of cortical, hippocampal and WB SUVs for TG and WT animals. Those for the TG animals demonstrate that after the differing initial uptakes, an equilibrium is reached where the [^{18}F]F-DPA$_N$ has a 1.5-fold higher uptake than the [^{18}F]F-DPA$_E$. A ratio greater that 1 is to be expected given the presence of specific uptake and the relative specific activities of the tracers. This higher uptake of radioactivity can also be seen in Figure 3. Although both [^{18}F]F-DPA$_N$ and [^{18}F]F-DPA$_E$ give highly significant differences between ROI/HYP ratios of TG and WT animals, inspection of these differences shows that in several brain regions, such as FC, PTC and HIPP, the difference is greater for [^{18}F]F-DPA$_N$.

The lack of specific binding in WT animals leads to higher peak uptake of both [^{18}F]F-DPA$_N$ and [^{18}F]F-DPA$_E$ compared to TG animals. However, due to the different injected masses, namely, the large amount of cold compound in the [^{18}F]F-DPA$_E$, the [^{18}F]F-DPA$_E$ activity in WT animals quickly drops, but the [^{18}F]F-DPA$_N$ activity decreases at a much slower rate. This difference in kinetics results in the [^{18}F]F-DPA$_N$/[^{18}F]F-DPA$_E$ SUV ratio graphs (Figure 4) initially peaking at around 1.5 but then decreasing to approximately 1. The final ratio of around 1 for the [^{18}F]F-DPA$_N$/[^{18}F]F-DPA$_E$ SUV of WT animals indicates that once an equilibrium has been reached, there is no difference between the uptake of [^{18}F]F-DPA$_N$ and [^{18}F]F-DPA$_E$ in WT animals. This observation is further corroborated by the ex vivo autoradiography ROI/HYP ratios, which are on approximately the same level for WT animals when imaging is performed with either [^{18}F]F-DPA$_N$ or [^{18}F]F-DPA$_E$.

In the case of the autoradiography ratios, the HYP was used as a reference region, since, as previously reported,[13] it is a region that is relatively free from pathology in the APP/PS1-21 mouse model. However, due to the close proximity of the HYP to the pituitary gland, the HYP cannot be used as a reference region for in vivo data.[13] Due to the higher sensitivity of the autoradiography imaging modality compared to in vivo PET and the use of a reference region, significant differences could be seen between TG and WT animals, in all the brain regions, when they are imaged with either [^{18}F]F-DPA$_N$ or [^{18}F]F-DPA$_E$.

Conclusions

Low A_m [^{18}F]F-DPA$_E$ was previously shown to be able to detect low-level inflammation in the APP/PS1-21 mouse model of AD.[13] The high A_m [^{18}F]F-DPA$_N$, presented herein, allows for a lower injected mass which in turn improves the ability to detect differences between healthy and diseased animals.

The comparison of the tracer product from the two different labelling strategies in the same animals demonstrated that the differing injected masses (38 ± 15 vs 0.34 ± 0.13 μg/kg), resulting from the two labelling

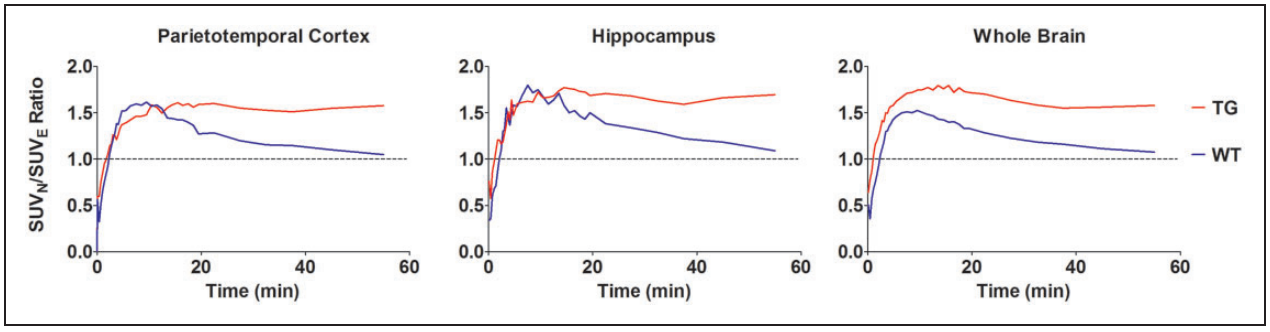

Figure 4. Ratios between [^{18}F]F-DPA$_N$ and [^{18}F]F-DPA$_E$ SUVs for TG and WT animals presented as a function of time. TG: transgenic; WT: wild type; SUV: standardized uptake value.

methodologies, have a pronounced effect on the washout profile and the shape on the TACs. The high A_m ($A_m = 990 \pm 150$ GBq/μmol, decay corrected to EOB) allows for a low injected mass (0.34 ± 0.13 μg/kg) which results in a lower "self-blocking" of the target by the non-radioactive portion of the tracer. Hence, there is a higher binding of the radioactive F-DPA in the brains of TG animals. Nevertheless, the low A_m [^{18}F]F-DPA$_E$ ($A_m = 9.0 \pm 2.9$ GBq/μmol, decay corrected to EOB) can still be used to detect significant differences between TG APP/PS1-21 and WT animals. However, in the case of diseases where the changes are more subtle use of the high A_m [^{18}F]F-DPA$_N$ would be more favourable.

Funding

The author(s) disclosed receipt of the following financial support for the research, authorship, and/or publication of this article: This study was financially supported by the European Community's Seventh Framework Programs FP7-PEOPLE-2012-ITN-RADIOMI-316882 and HEALTH-F2-2011-278850 (INMiND), by a clinical grant from the Turku University Hospital (EVO, grant no 13250), and by the Academy of Finland (grant nos. 266891 and 310962).

Acknowledgements

We would like to thank Prof. Gouverneur and her research group at the University of Oxford for their supervision and assistance during T. Keller's secondment there during which the synthesis of the precursor was carried out.

Declaration of conflicting interests

The author(s) declared no potential conflicts of interest with respect to the research, authorship, and/or publication of this article.

Authors' contribution

The specific contributions of each author are as follows: TK carried out the chemistry for the synthesis of precursors. TK, AK, SF, JR, and OS contributed to the radiochemistry. TK, FRL-P, AK, JT, and MH-S acquired and analysed the preclinical data and prepared the manuscript. ST and TK performed the statistical analyses. FD, JOR, MH-S and OS contributed to the conception and design of the study and have critically contributed to and revised the manuscript. All the authors discussed the experimental results and commented on the manuscript.

References

1. Forsback S, Eskola O, Haaparanta M, et al. Electrophilic synthesis of 6-[^{18}F]fluoro-L-DOPA using post-target produced [^{18}F]F_2. *Radiochi Acta* 2008; 96: 845–848.
2. Fujimura Y, Ito H, Takahashi H, et al. Measurement of dopamine D_2 receptors in living human brain using [^{11}C]raclopride with ultra-high specific radioactivity. *Nucl Med Biol* 2010; 37: 831–835.
3. Bégué J-P and Bonnet-Delpon D. Recent advances (1995–2005) in fluorinated pharmaceuticals based on natural products. *J Fluor Chem* 2006; 127: 992–1012.
4. Müller K, Faeh C and Diederich F. Fluorine in pharmaceuticals: looking beyond intuition. *Science* 2007; 317: 1881–1886.
5. Wang J, Sánchez-Roselló M, Aceña JL, et al. Fluorine in pharmaceutical industry: fluorine-containing drugs introduced to the market in the last decade (2001 – 2011). *Chem Rev* 2014; 114: 2432–2506.
6. Blessing G, Coenen H, Franken K, et al. Production of [^{18}F]F_2, H^{18}F and $^{18}F_{aq}^-$ using the ^{20}Ne(d, α)^{18}F process. *Int J Radiat Appl Instrum Part A* 1986; 37: 1135–1139.
7. Hess E, Blessing G, Coenen H, et al. Improved target system for production of high purity [^{18}F]fluorine via the ^{18}O(p,n)^{18}F reaction. *Appl Radiat Isotop* 2000; 52: 1432–1440.
8. Bergman J and Solin O. Fluorine-18-labeled fluorine gas for synthesis of tracer molecules. *Nucl Med Biol* 1997; 24: 677–683.
9. Krzyczmonik A, Keller T, Kirjavainen AK, et al. Vacuum ultraviolet photon-mediated production of [F-18]F_2. *J Label Compd Radiopharm* 2017; 60: 186–193.
10. Eskola O, Forsback S, Bergman J, et al. Electrophilic Synthesis of [^{18}F]EF_5, a Radiotracer for Imaging of Tumor Hypoxia. *Eur J Nucl Med Mol Imaging* 2005; 32: S53.
11. Forsback S, Marjamaki P, Eskola O, et al. [^{18}F]CFT synthesis and binding to monoamine transporters in rat. *EJNMMI Res* 2012; 2: 3.
12. Keller T, Krzyczmonik A, Forsback S, et al. Radiosynthesis and Preclinical Evaluation of [^{18}F]F-DPA, A Novel Pyrazolo[1,5a]pyrimidine Acetamide TSPO Radioligand, in Healthy Sprague Dawley Rats. *Mol Imaging Biol* 2017; 19: 736–745.
13. Keller T, López-Picón FR, Krzyczmonik A, et al. [^{18}F]F-DPA for the detection of activated microglia in a mouse model of Alzheimer's disease. *Nucl Med Biol* 2018; 67: 1–9.
14. Wang L, Cheng R, Fujinaga M, et al. A facile radiolabeling of [^{18}F]FDPA via spirocyclic iodonium ylides: preliminary PET imaging studies in preclinical models of neuroinflammation. *J Med Chem* 2017; 60: 5222–5227.
15. Zischler J, Kolks N, Modemann D, et al. Alcohol-enhanced Cu-mediated radiofluorination. *Chem Eur J* 2017; 23: 3251–3256.
16. Caillé F, Cacheux F, Damont A, et al. [^{18}F]F-DPA, a new PET tracer to image TSPO in neuroinflammation. *J Label Compd Radiopharm* 2017; 60: S414.
17. Preshlock S, Calderwood S, Verhoog S, et al. Enhanced copper-mediated ^{18}F-fluorination of aryl boronic esters provides eight radiotracers for PET applications. *Chem Comm* 2016; 52: 8361–8364.
18. Gamache R, Waldmann C and Murphy J. Copper-mediated oxidative fluorination of aryl stannanes with fluoride. *Org Lett* 2016; 18: 4522–4525.
19. Takkinen J, López-Picón FR, Keller T, et al. Brain energy metabolism and neuroinflammation in ageing APP/PS1-21 mice using longitudinal ^{18}F-FDG and

^{18}F-DPA-714 PET imaging. *J Cereb Blood Flow Metab* 2017; 37: 2870–2882.
20. Radde R, Bolmont T, Kaeser SA, et al. Aβ42-driven cerebral amyloidosis in transgenic mice reveals early and robust pathology. *EMBO Rep* 2006; 7: 940–946.
21. Rupp NJ, Wegenast-Braun BM, Radde R, et al. Early onset amyloid lesions lead to severe neuritic abnormalities and local, but not global neuron loss in APPPS1 transgenic mice. *Neurobiol Aging* 2011; 32: 2324.e1–2324.e6.
22. Pascali C, Luthra SK, Pike VW, et al. The radiosynthesis of [18F]PK 14105 as an alternative radioligand for peripheral type benzodiazepine binding sites. *Appl Radial Isot* 1990; 41: 477–482.
23. Imaizumi M, Briard E, Zoghbi SS, et al. Kinetic evaluation in nonhuman primates of two new PET ligands for peripheral benzodiazepine receptors in brain. *Synapse* 2007; 61: 595–605.
24. Imaizumi M, Briard E, Zoghbi SS, et al. Brain and whole-body imaging in nonhuman primates of [^{11}C]PBR28, a promising PET radioligand for peripheral benzodiazepine receptors. *Neuroimage* 2008; 39: 1289–1298.
25. Eberl S, Katsifis A, Peyronneau MA, et al. Preclinical in vivo and in vitro comparison of the translocator protein PET ligands [^{18}F]PBR102 and [^{18}F]PBR111. *Eur J Nucl Med Mol Imaging* 2017; 44: 296–307.
26. Zanotti-Fregonara P, Zhang Y, Jenko KJ, et al. Synthesis and Evaluation of Translocator 18 kDa Protein (TSPO) positron emission tomography (PET) radioligands with low binding sensitivity to human single nucleotide polymorphism rs6971. *ACS Chem Neurosci* 2014; 5: 963–971.
27. Samson Y, Hantraye P, Baron JC, et al. Kinetics and displacement of [^{11}C]RO 15-1788, a benzodiazepine antagonist studied in human brain in vivo by positron tomography. *Eur J Pharmacol* 1985; 110: 247–251.
28. Delforge J, Syrota A, Bottlaender M, et al. Modeling analysis of [^{11}C]flumazenil kinetics studied by PET: application to a critical study of the equilibrium approaches. *J Cereb Blood Flow Metab* 1993; 13: 454–468.